Density Functional Calculations on the Conversion of Azide and Carbon Monoxide to Isocyanate and Dinitrogen by a Nickel to Sulfur Rebound Mechanism

Yubo Fan and Michael B. Hall*[a]

Dedicated to the memory of our friend and colleague Dieter Sellmann

Abstract: Density functional calculations (B3LYP & BP86) on a model system for the reaction between carbon monoxide and $[Ni(N_3)('S_3')]^-$ ($'S_3'^{2-}$ = bis(2-mercaptophenyl)sulfide (2−)) predict a three-step mechanism. First, CO attacks the nickel to generate a pseudo "square-pyramidal" complex, in which CO, N_3^-, and two sulfides are basal and the central S atom of the $'S_3'^{2-}$ ligand backs away from Ni to form a weak Ni–S apical bond. Then, CO inserts into the Ni–N bond and the weak apical Ni–S bond rebounds to its original strength as the nickel forms a square-planar intermediate. Finally, in a one-step process N_2 leaves as the remaining N atom and carbonyl rearrange to produce the nickel isocyanate product $[Ni(NCO)('S_3')]^-$.

Keywords: azides · density functional calculations · nickel · rearrangement · S ligands

Introduction

Sulfur ligands play a major role in biological systems, especially in metalloenzymes such as dehydrogenases and hydrogenases.[1,2] A number of multidentate sulfur ligands have been synthesized and their metal complexes prepared and studied as enzyme active-site models.[3,4]

Recently, Sellmann and co-workers reported a series of reactions between CO, CO_2, SO_2, and the monodentate ligands N_3^-, $N(SiMe_3)_2^-$ on nickel bound to a tridentate sulfur ligand, bis(2-mercaptophenyl)sulfide dianion ($'S_3'^{2-}$) (Scheme 1).[3a] Sellmann et al. suggested a mechanism (Scheme 2),[3a] in which the incoming ligand (CO for example) forms a "square-pyramidal" five-coordinate intermediate by binding in the apical site. The incoming ligand then inserts into the nickel-monodentate-ligand bond and rearranges to a square-planar structure which then eliminates N_2.

To examine the role the $'S_3'^{2-}$ ligand plays in the reaction and to understand the mechanism, density functional theory (DFT) calculations have been carried out on the reaction of $[Ni('S_3')(N_3)]^-$ and CO to form $[Ni('S_3')(NCO)]^-$ and N_2 with a simplified version of Sellmann's ligand, in which $'S_3'^{2-}$ is modeled by bis(2-mercaptovinyl)sulfide dianion. Additionally, some species were examined by using the exact ligand. The reaction coordinate has been searched carefully and several intermediates and transition states (TS) has been located. A detailed mechanism and the various conformations of reactants and intermediates will be discussed.

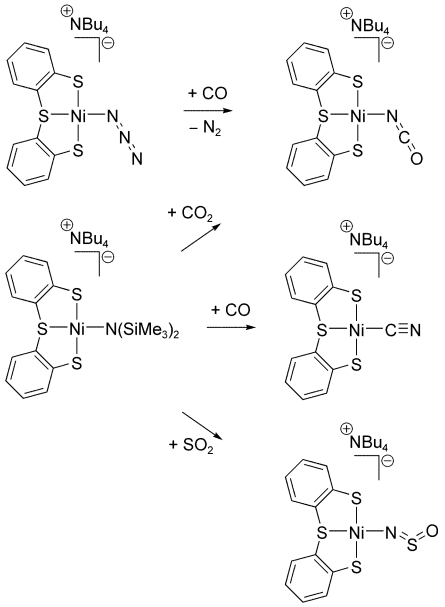

Scheme 1.

[a] Dr. Y. Fan, Prof. Dr. M. B. Hall
Chemistry Department, Texas A&M University
College Station, TX 77843-3255 (USA)
Fax: (+1) 979-845-2971
E-mail: mbhall@tamu.edu

 DOI: 10.1002/chem.200304840

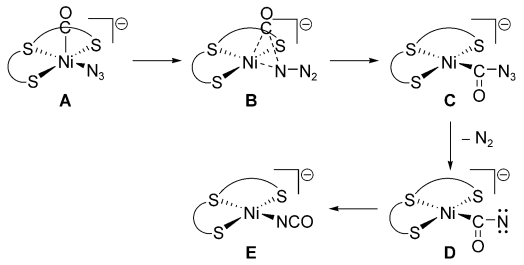

Scheme 2.

Computational Methods

Most of the calculations have been carried out using the Gaussian 98[5] implementation of B3LYP [Becke three-parameter exchange functional (B3)[6] and the Lee–Yang–Parr correlation functional (LYP)[7]] and BP86 [Becke's 1988 exchange functional (B)[8] and Perdew's correlation functional (P86)[9]] density functional theories.[10] A modified version of Hay and Wadt's LANL2DZ[11] with the two outermost p functions replaced by a new function with a (41) split[12] is used for nickel and an f-polarization function[13] is also added. The 6-31G* basis sets are utilized for all the sulfur, carbon, nitrogen, oxygen, and hydrogen atoms.[14] This combination of basis sets is defined as BS-I. For the intermediates and transition states in the reaction, both open shell (triplet) and closed shell (singlet) calculations have been run at the B3LYP/BS-I level, while BP86/BS-I only has been carried out for the closed-shell ones. All structures were fully optimized, and analytical frequency calculations were performed on each structure to ensure a minimum or transition state was achieved. Zero-point energy was calculated and thermodynamic functions were computed for 298.15 K and 1 atm.

To check the possibility of error from medium-size basis sets BS-I, B3LYP single-point energy (SPE) calculations have been carried out in BS-II defined as 6-311G**[15] on all elements except nickel, for which the same basis set as in BS-I was used. Moreover, the basis set BS-III, defined as SDD[16] for Ni and 6-31+G*[14] for all other elements, was used to reoptimize the reactant and product complex analogues with frequency analyses. PCM model[17] has been used to estimate the solvent effects (THF) with B3LYP/BS-I SPE on the geometries optimized in vacuum.

Additionally, B3PW91,[6,18] BLYP,[8,7] BPW91,[8,18] and PBE[19] are also used and frequency analysis of certain complexes to estimate the degree of the overstabilization of triplets by the hybrid DFT-B3LYP method.

Table 1. Singlet–triplet gaps for species **1**–**4**.

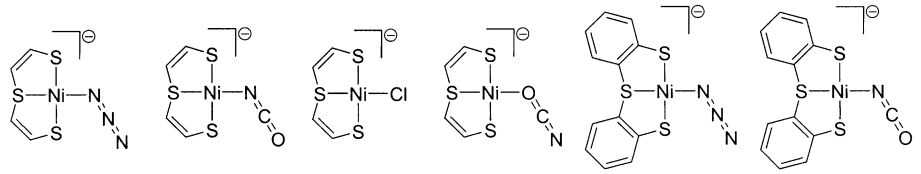

Species	DFT/basis sets	ΔE [kcal mol^{-1}]	ΔE_0 [kcal mol^{-1}]	$\Delta H°$ [kcal mol^{-1}]	$\Delta G°$ [kcal mol^{-1}]	$\Delta S°$ [cal K^{-1} mol^{-1}]
1a	B3LYP/BS-I	5.46	5.89	5.50	8.39	−9.70
1a	BLYP/BS-I	−1.01	−0.61	−0.97	1.34	−7.75
1a	BP86/BS-I	−2.74	−2.30	−2.68	−0.37	−7.75
1a	B3PW91/BS-I	5.08	5.53	5.12	7.87	−9.21
1a	BPW91/BS-I	−1.95	−1.52	−1.89	0.42	−7.76
1a	PBE/BS-I	−2.84	−2.39	−2.78	−0.41	−7.92
2	B3LYP/BS-I	6.37	6.87	6.44	9.10	−8.95
2	BLYP/BS-I	−0.77	−0.30	−0.72	1.81	−8.47
2	BP86/BS-I	−2.72	−2.22	−2.65	−0.11	−8.52
2	B3PW91/BS-I	5.92	6.43	5.99	8.69	−9.04
2	BPW91/BS-I	−1.87	−1.38	−1.81	0.73	−8.52
2	PBE/BS-I	−2.78	−2.28	−2.72	−0.16	−8.58
1a	B3LYP/BS-III	8.87	9.23	8.87	11.36	−8.35
2	B3LYP/BS-III	9.87	10.24	9.91	11.75	−6.16
3	B3LYP/BS-I	8.82	9.16	8.82	11.04	−7.47
4	B3LYP/BS-I	6.61	7.06	6.67	9.66	−10.03
1a′	B3LYP/BS-I	4.86	5.23	4.37	8.44	−13.66
1a′	BP86/BS-I	−3.08	−2.56	−2.89	−0.71	−7.32
2′	B3LYP/BS-I	5.49	6.09	5.69	8.45	−9.26
2′	BP86/BS-I	−3.01	−2.43	−2.81	−0.29	−8.44

Results and Discussion

Comparison of singlets and triplets of known species

Both singlets and triplets of some known Ni–S complexes, or close analogues, are calculated because two-state reactivity often exists in transition-metal (bio)inorganic or organometallic reactions.[20] The calculated singlet–triplet gaps for **1**–**4** are listed in Table 1.

The optimizations show that the singlet structures are square-planar with slight distortions toward tetrahedral, whereas the triplets take a nearly tetrahedral geometry. As listed in Table 1, all singlet structures, which are calculated with B3LYP theory, are less stable than the corresponding triplets. However, the singlet structures are consistent with the experimental crystal structures.[3] Moreover, the NMR experiments appear to involve only singlet states. Thus, the B3LYP functional must overestimate the stability of the triplet states. In contrast, the pure DFT functional, such as BP86, BLYP, BPW91, and PBE, indicate that the singlets are more stable by 1~3 kcal mol^{-1} in enthalpy and nearly the same stability as the triplets in free energy. Another hybrid DFT-B3PW91 also gives the results similar to those of B3LYP. Interestingly, the singlet–triplet (S–T) gap becomes larger as the better basis set BS-III is combined with B3LYP to reoptimize **1a** and **2**. Again BP86 changes the sign of the S–T gap for **1a**′ and **2**′ compared to B3LYP, but here the gap (−0.71 and −0.29) for the free energy would be barely large enough to maintain all of **1a**′ and **2**′ in the singlet form.

In transition-metal complexes, the stability of high-spin states is commonly overestimated by hybrid functionals.[21] Salomon et al. calculated some iron–sulfur complexes by a

modified version of B3LYP (B3LYP*),[22] in which the HF exchange is reduced from 20% to 15%. However, this modification is still not good enough to deal with these NiS_3 complexes because here there is a large geometric change from the singlet's square-planar into the triplet's tetradredal geometry. Even BLYP, in which HF exchange is not included at all, cannot deal with the singlet–triplet gap correctly (Table 1).

Thus, corrections of about 10.00 kcal mol^{-1} for $\Delta H°$ and $\Delta G°$ are reasonable and necessary for all triplets based on B3LYP/BS-I calculations. All the B3LYP/BS-I energies reported are raised by 10.0 kcal mol^{-1} for the triplet states.

Closed-shell (singlet) mechanism (B3LYP/BS-I)Overall reaction: Our calculations, which are based on the closed-shell model, indicate a three-step mechanism (Scheme 3): 1) the formation of the pseudo "square-pyramidal" intermediate (**9a** or **9b**), 2) the insertion of CO into nickel–azide bond and, 3) the rearrangement of carbonyl azide to form isocyanate and eliminate N_2. The key species in the reaction path, the reaction coordinates, their structural parameters, and their relative energies and thermodynamic functions are shown in Figure 1, Figure 2, Table 2, and Table 3, respectively.

Overall, the nickel-mediated transformation of azide and carbon monoxide into isocyanate and dinitrogen is a very exothermic reaction, $\Delta H^{\circ} = \sim -60$ kcal mol^{-1}. The relative energies of the intermediates are very close to that of the reactants as most of the energy release comes from formation of N_2, which occurs last in the reaction. Carbon monoxide can react with nickel from either side of the Ni–S_3 plane. The formation of **9** occurs readily through fairly low barriers. The barriers for the next two steps of the reaction are low to moderate (Table 2). These sequential activation enthalpies imply a moderate reaction rate at room temperature or even lower.

Reactant: The nickel azide reactant has two C_s symmetry conformations, **1a** and **1b** (see Scheme 4). Because the two terminal thiolate-sulfur atoms are tipped in the same direction, the NiS_3 "plane" looks like a shell, and the two sides of the NiS_3 "plane" can be differentiated as *endo* and *exo*. Conformation **1a** is more stable than **1b** by only 1.63 kcal mol^{-1} (ΔH°) and the transition state (**1-TSa**) for rotation about the Ni–N bond, is only above **1b** by 1.5 kcal mol^{-1} in free energy. Thus, the rotation of azide is rapid under the reaction conditions. Additionally, another transition state (**1-TSb**) is also found between **1a** and **1b** and the process of

Table 2. The B3LYP/BS-I changes of enthalpy and Gibbs free energy [kcal mol^{-1}] for the singlet species in Scheme 3.

Species	$\Delta H^{\circ(+)}$ [kcal mol^{-1}]	$\Delta G^{\circ(+)}$ [kcal mol^{-1}]	Species	$\Delta H^{\circ(+)}$ [kcal mol^{-1}]	$\Delta G^{\circ(+)}$ [kcal mol^{-1}]
1a+CO	2.29	−4.11	**1b**+CO	3.95	−2.84
5a	0.00	0.00	**5b**	1.44	1.77
6-TSa	8.81	12.15	**6-TSb**	6.89	10.59
9a	1.42	5.07	**9b**	0.01	3.40
10-TSa	16.94	21.29	**10-TSb**	7.30	11.42
11a	−0.36	3.75	**11b**	−0.17	3.57
12-TSa	14.97	18.93	**12-TSb**	14.44	18.31
2+N_2	−66.15	−72.38	**2**+N_2	−66.15	−72.38

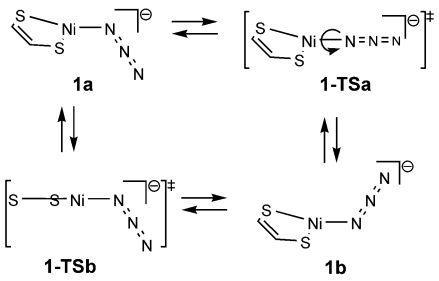

Scheme 4. The third S of $'S_3'^{2-}$ is eclipsed in **1a**, **1b**, and **1-TS**s.

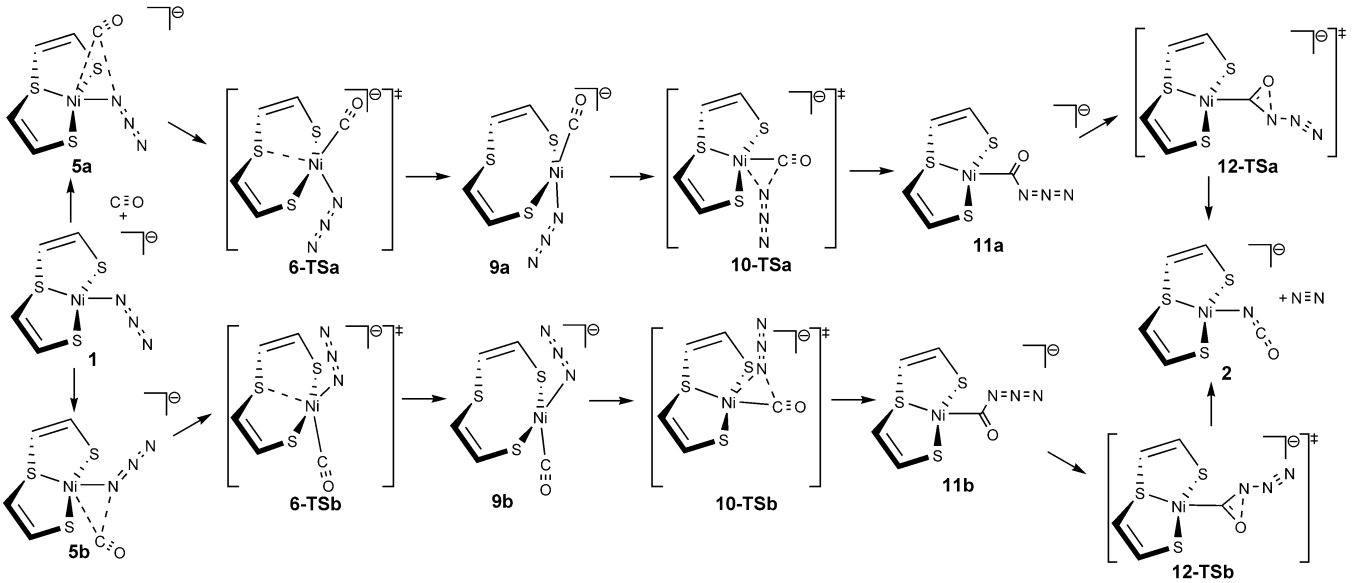

Scheme 3. Singlet mechanism.

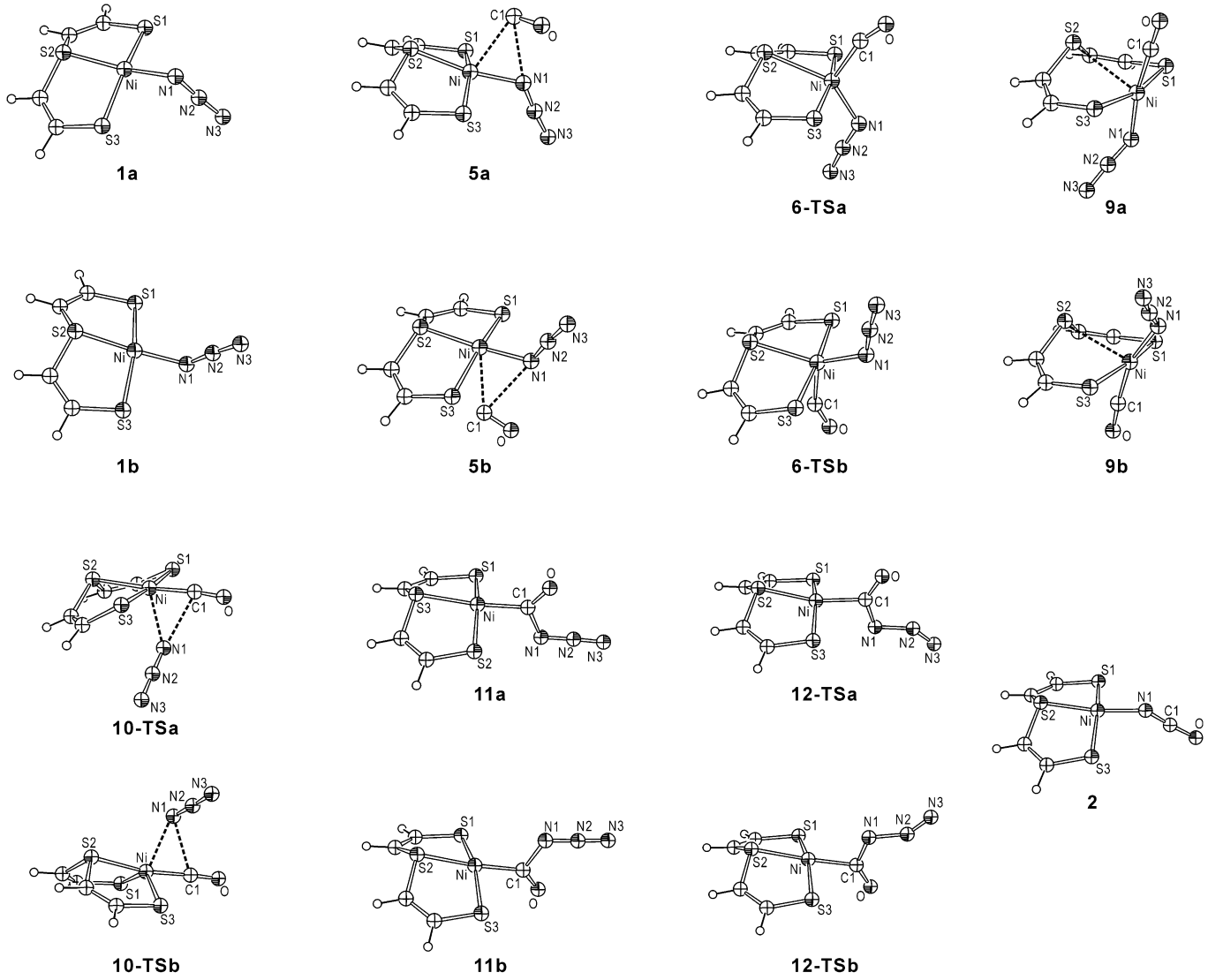

Figure 1. The B3LYP/BS-I geometries of the species in the singlet mechanism.

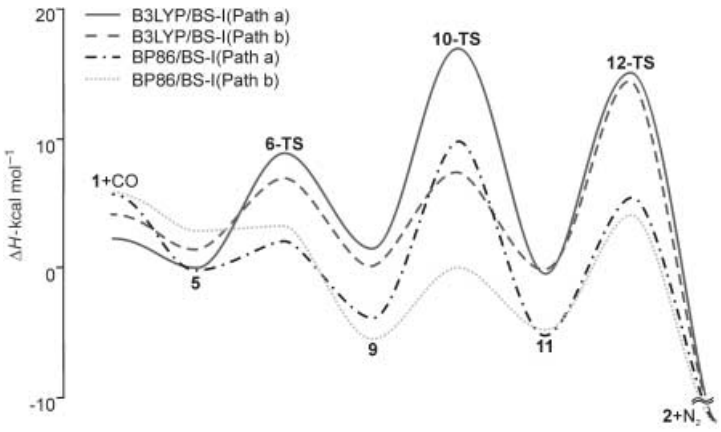

Figure 2. The comparison of the energetics calculated at the B3LYP level with those calculated at the BP86 level in the singlet mechanism.

1a→**1-TSb**→**1b** involves flattening and refolding the NiS_3 framework. In this transition state (**1-TSb**), Ni, three S atoms, and the coordinated N atom are almost planar. The S2-Ni-N1 bond angle is 177.6° and the angle between planes of Ni-S2-S1 and Ni-S2-S3 is 0.0°. The barrier for this refolding path is about 16 kcal mol^{-1} higher than that for the rotation. However, this refolding may be more important in complexes with very bulky ligands.

Weak complexes of reactants: Carbon monoxide can approach Ni from either the *exo* or *endo* side. Two weak complexes (**5a** and **5b**) of **1** and CO are located and they are about 3 kcal mol^{-1} more stable than the reactants. The weak adducts (**5a** and **5b** in Figure 1) of **1** and CO seem to be bound through a π–π interaction with a long Ni–C bond. Although the failure of DFT methods to properly account for dispersion effects may make this adduct more stable than the calculated energies would suggest, DFT methods often produce a reasonable geometry, in spite of their poor energy. Adducts **5** have calculated CO vibrational frequencies that are 19 cm^{-1} lower than that calculated for free CO (Table 4). This difference compares well with the 14 cm^{-1} shift observed by Sellmann et al. for his proposed labile

Table 3. B3LYP/BS-I structure parameters for singlet species in Figure 1.

Structure parameters[a]	**1a**	**5a**	**6-TSa**	**9a**	**10-TSa**	**11a**	**12-TSa**	**2**
Ni–S2	2.256	2.256	2.549	2.972	2.288	2.304	2.302	2.240
Ni–S1	2.286	2.285	2.324	2.340	2.300	2.278	2.278	2.289
Ni–S3	2.286	2.291	2.324	2.300	2.296	2.278	2.278	2.289
Ni–N1	1.895	1.898	1.928	1.887	2.344	2.846	2.618	1.876
N1–N2	1.210	1.210	1.210	1.208	1.200	1.235	1.497	
N2–N3	1.161	1.160	1.161	1.160	1.172	1.143	1.128	
C1–N1		3.184	3.350		2.704	1.513	1.322	1.201
Ni–C1		3.114	1.965	1.798	1.808	1.874	1.929	
C1–O		1.140	1.147	1.148	1.147	1.209	1.226	1.202
S2-Ni-N1	168.5	169.4	142.0	107.5	104.3		167.0	169.2
S2-Ni-C1		95.3	99.2	81.1	175.5	172.1	163.9	
S1-Ni-S3	159.5	158.7	164.2	165.7	175.9	160.3	159.4	159.7
N1-N2-N3	174.6	174.6	174.9	174.7	178.2	177.5	142.9	
Structure parameters[a]	**1b**	**5b**	**6-TSb**	**9b**	**10-TSb**	**11b**	**12-TSb**	**2**
Ni–S2	2.251	2.247	2.483	2.833	2.245	2.299	2.307	2.240
Ni–S1	2.285	2.283	2.295	2.338	2.343	2.279	2.275	2.289
Ni–S3	2.285	2.286	2.295	2.302	2.355	2.279	2.275	2.289
Ni–N1	1.911	1.910	1.925	1.892	2.297	2.765	2.493	1.876
N1–N2	1.212	1.212	1.212	1.209	1.210	1.233	1.478	
N2–N3	1.162	1.162	1.162	1.160	1.165	1.145	1.132	
C1–N1		3.572	3.422		2.356	1.548	1.330	1.201
Ni–C1		3.092	2.077	1.799	1.788	1.876	1.934	
C1–O		1.141	1.147	1.149	1.150	1.200	1.220	1.202
S2-Ni-N1	173.4	173.7	146.3	104.3	101.2		144.1	169.2
S2-Ni-C1		98.4	96.2	94.1	170.3	173.5	176.0	
S1-Ni-S3	160.6	162.4	173.3	164.9	136.2	160.1	161.7	159.7
N1-N2-N3	174.4	174.5	174.5	174.7	177.2	178.7	142.6	

[a] Bond lengths in Å, bond angles in °.

Table 4. Vibrational frequencies of CO[a] for certain singlet species in Figure 1 and 3.

Species	B3LYP	BP86	Species	B3LYP	BP86
5a	2189.3	1975.4	**5b**	2177.9	1987.8
6-TSa	2102.9	1977.6	**6-TSb**	2101.1	1954.4
9a	2121.8	2011.9	**9b**	2115.1	2006.5
10-TSa	2125.9	1996.3	**10-TSb**	2106.1	1970.5
11a	1760.6	1699.3	**11b**	1800.9	1739.5
5ta	2183.8		**5tb**	2191.1	

[a] ν(free CO) = 2208.6 cm^{-1}(B3LYP) or 2116.5 cm^{-1} (BP86).

five-coordinate species **A**, although the calculated structure is quite different form his hypothesized one.

The counterpoise calculations[23] find that **5a** and **5b** have BSSE of 3–3.5 kcal mol^{-1}. Although BSSE is mainly responsible for the calculated stabilities of **5a** and **5b**, it is still chemically reasonable that in the condensed phase weak complexes form before the reaction occurs.

First step: This step leads from the weak reactant complexes, **5a** and **5b**, through **6-TS**s to the "square-pyramidal" intermediate **9a** and **9b**, respectively (Figure 1, Table 2 and Table 3).

In the transition states (**6-TSa** and **6-TSb**) the azide moves away to a position *trans* to the incoming CO, while the Ni–S2 bond weakens significantly to form the "square-pyramidal" intermediates, **9a** and **9b**, in which CO, N_3^-, S1, and S3 are on the base of the square pyramid, and S2 is weakly bound at the apex. Compared with **1**, the bond length of Ni–S2 has increased by 0.6–0.7 Å in **9**. Since the azide rotates about the Ni–N bond to stay in the pyramidal basal plane, symmetries of **9** are reduced to C_1.

Second step: In this step's transition states, **10-TSa** and **10-TSb**, N_3^- migrates from Ni to CO and in doing so the Ni–N1 bond lengthens by more than 0.4 Å, while the C1–N1 bond decreases by ~1 Å. Apparently, the apical S (S2) in **9a** and **9b** helps N_3^- migration by enhancing the Ni–S2 bond, which shortens by 0.6–0.7 Å, so that the binding between Ni and N_3^- is weakened and carbonyl simultaneously moves to the *trans* position to maintain the d^8 square-planar geometry for carbonyl azide intermediates **11a** and **11b**. Interestingly, as the Ni–S2 rebounds, the square-planar geometry is almost completely reformed in the transition states.

The intermediates **11a** and **11b** are nickel square-planar carbonyl azide complexes and the Ni–C1 bond, which is 0.08 Å longer than those in **9a** and **9b**, is a single bond. Moreover, four nearly isoenergetic conformations are found for **11** and all of them are C_s symmetry (Scheme 5). They readily transform among themselves by rotating about the C–N and Ni–C bonds.

Third step: Finally, the nickel carbonyl azide complex **11** rearranges to produce the product, the nickel isocyanate complex **2**, by releasing a molecule of N_2. The transition states **12-TSa** and **12-TSb** are very early as the products, **2** and N_2, are over 60 kcal mol^{-1} more stable than **11**. Interestingly, N_2 leaving and the rearrangement to isocyanate appear synchronous not stepwise. Intrinsic reaction (IRC) calcula-

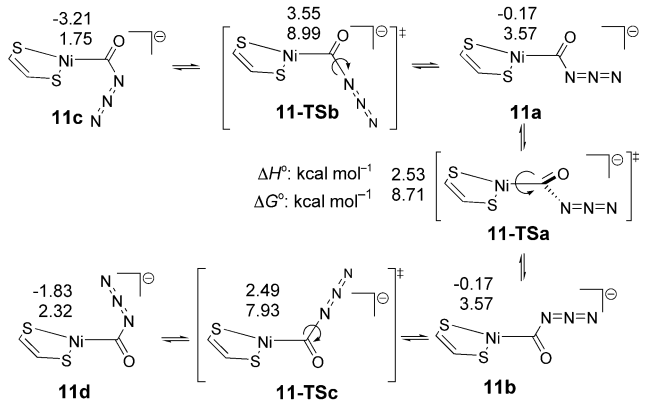

Scheme 5. Isoenergetic conformations found for **11**.

tions[24] were performed for **12-TSb** and it is confirmed that **12-TSb** is the transition state between **11b** and **2** plus N_2.

Although the unstable carbonyl nitrene intermediate **13**, which is similar to **D** in the proposed mechanism has been located (Scheme 6 and Figure 3), this intermediate is 2.7 kcal mol^{-1} (ΔH) less stable than the transition state (**12-TSb**) on the synchronous route to the products. Species **13** appears to be more like an oxazirene (three-membered heterocycle) than a carbonyl nitrene as there is a very strong N–O interaction in **13**. Even though the free energy of **13** and N_2 is lower than that for **12-TSb**, the expected transition state between **11b** and **13** would be higher in energy than **6-TS** because the barrier for this type of dissociation reaction depends on the ΔH for dissociation. All attempts to find this expected transition state from **11b** to **13** failed; whenever the N1–N2 bond is lengthened in **11b**, N1 always inserts into the Ni–C bond to form the product. This behavior is consistent with the higher energy of the oxazirene complex, **13**. The barrier for the rearrangement of **13** to form the product is only 4 kcal mol^{-1} (**14-TS**). Thus, **13** appears to be a high-energy isomer of the product **2**, but not on the reaction path from **11b**.

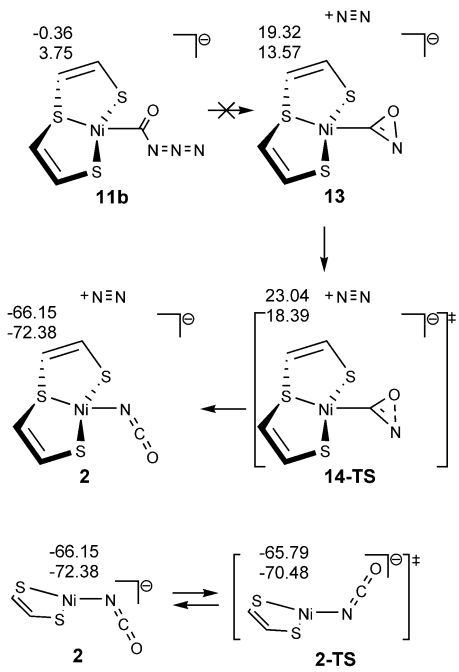

Scheme 6.

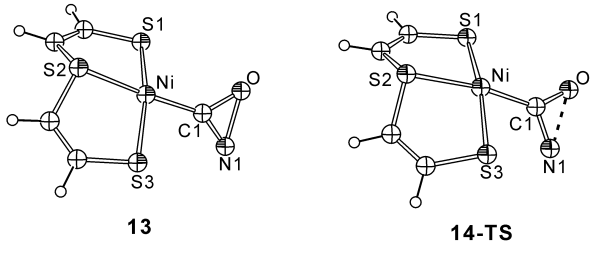

Figure 3. The B3LYP/BS-I geometries of the singlet species in the dissociation mechanism.

Unlike the nickel azide complex (**1a** and **1b**), **2**, which has C_s symmetry, is the only stable conformation for the nickel isocyanate complex. The species, in which the isocyanate group is rotated by 180° about the Ni–N bond, is a transition state (**2-TS**) rather than another minimum and it is only 0.37 kcal mol^{-1} ($\Delta H^{\neq}$) higher than **2**.

Path a versus path b: Figure 2 summarizes the energetics of this reaction on the singlet surface. Path b is generally more favorable than path a, and in path b the third step would be rate-determining. The BP86 barriers are significantly lower than these from the B3LYP calculations. Considering the experimental conditions (room temperature for 17 h), the barriers from B3LYP calculations would appear to be more accurate.

Open-shell (triplet) mechanism (B3LYP/BS-I)

Overall reaction: Although ΔH° for the reaction based on triplet potential energy surface, which is -59 kcal mol^{-1}, is similar to that of the closed-shell mechanism, the triplet mechanism includes four steps (Scheme 7, Figure 4 and Figure 5). First, a five-coordinate intermediate forms by CO attack on the complex. Second, the carbonyl moves *trans* to the thioetheric sulfur atom and the azide moves to the *cis* position by a swaying vibrational mode. Then, the azide migrates to the carbonyl to form the carbonyl azide complex. At last, the carbonyl azide group rearranges to produce the isocyanate complex by releasing one molecule of N_2. The energy barriers for the first three steps are low to moderate while the last step is highly energetic (estimated to be ~13 kcal mol^{-1} higher than that for the corresponding step in the singlet mechanism). In addition, the four-coordinate species in the triplet mechanism are more tetrahedral than those in the singlet one. Some key species' structural parameters and their relative energies and thermodynamic functions are shown in Table 5 and Table 6, respectively.

Weak complexes of reactants: Two weak complexes (**5ta** and **5tb**) of **1t** and CO are also located and they are 1.4–2.5 kcal mol^{-1} more stable than the reactants without BSSE correction. Their formation energies are similar to those in the singlet mechanism. CO seems to interact with Ni, N1,

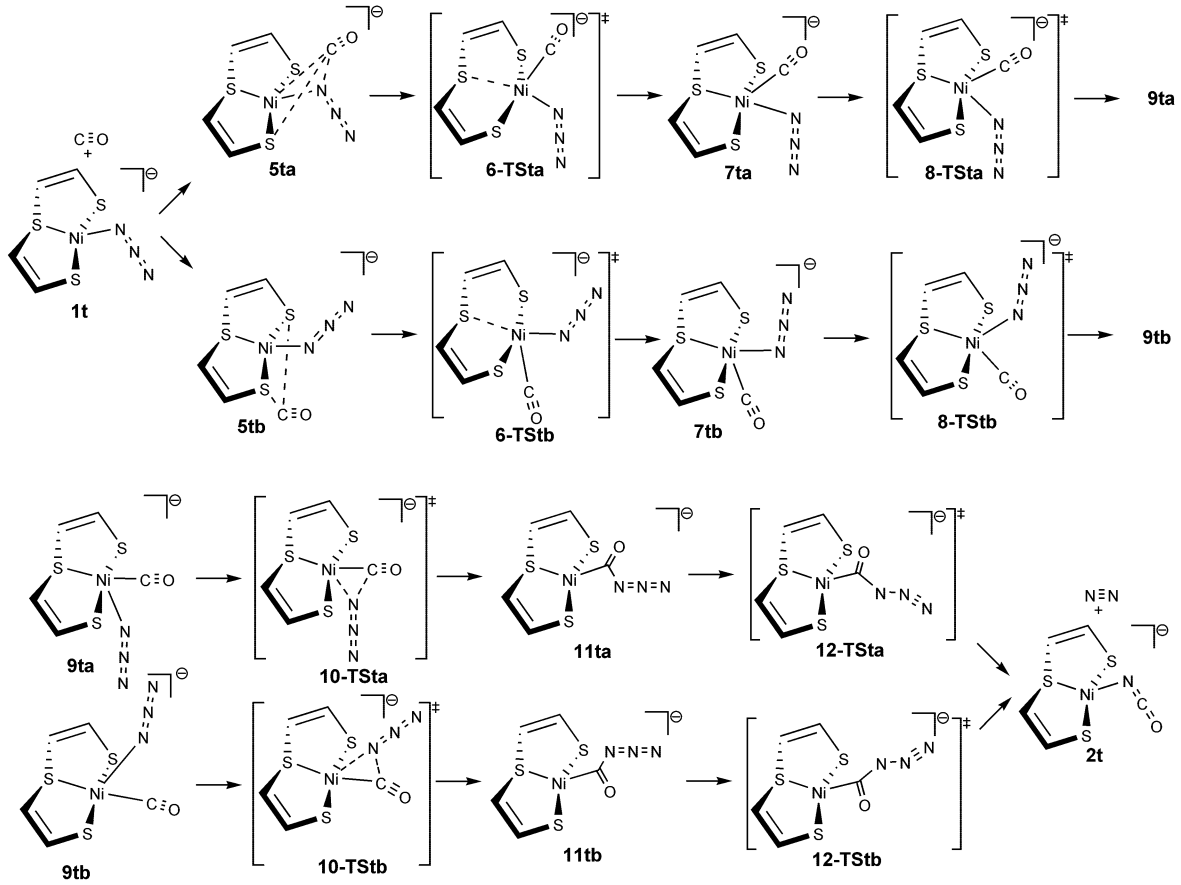

Scheme 7. Triplet mechanism.

Table 5. The B3LYP/BS-I changes of enthalpy and Gibbs free energy [kcal mol^{-1}] for the species in Scheme 7.[a]

Species	$\Delta H^{\circ(+)}$	$\Delta G^{\circ(+)}$	Species	$\Delta H^{\circ(+)}$	$\Delta G^{\circ(+)}$
1t+CO[a]	5.37	−7.57	**1t**+CO	5.37	−7.57
5ta	2.87	−2.41	**5tb**	3.99	−2.81
6-TSta	3.51	2.54	**6-TStb**	7.13	4.97
7ta	3.69	0.87	**7tb**	4.81	2.25
8-TSta	12.67	10.40	**8-TStb**	6.45	4.63
9ta	12.03	9.71	**9tb**	2.09	−1.25
15-TSt	20.25	17.52	**10-TStb**	13.99	12.48
11ta	15.48	13.31	**11tb**	14.56	11.96
12-TSta	27.01	24.81	**12-TStb**	27.45	25.62
2t+N_2	−64.01	−76.56	**2t**+N_2	−64.01	−76.56

[a] All energies are compared to **5a** + 10 kcal mol^{-1}.

and S3 atoms in **5ta**, whereas it is only bound to S1 and S2 in **5tb**.

First step: The energy barriers (**6-TSta** and **6-TStb**) for this step are at least 3 kcal mol^{-1} lower than those of the singlet mechanism. The activation enthalpy ($\Delta H^{\neq}$) is 0.64 kcal mol^{-1} for the attack of CO from the *exo* side and 3.14 kcal mol^{-1} from the *endo* side.

The intermediates (**7ta** and **7tb**) also have geometries between square-pyramidal and trigonal bipyramidal. **7ta** is closer to trigonal bipyramidal and **7tb** is closer to square-pyramidal as the angles of S1-Ni-S3 are 142.8° and 164.4° for **7ta** and **7tb**, respectively (Figure 4 and Table 6). The azide ligand remains *trans* to the thioether-S, and the CO remains *cis* to the S, while in **9a** and **9b** the azide and the carbonyl are *trans*. Intermediates **7ta** and **7tb** are only 1 kcal mol^{-1} less stable than the reactant adducts **5ta** and **5tb**, respectively.

Second step: Unlike the singlet mechanism, the square-pyramidal intermediates, **7ta** and **7tb**, cannot react to form the carbonyl azide intermediates, **11ta** and **11tb**, directly. They must rearrange to the other five-coordinate intermediates (**9ta** and **9tb**) first.

The geometries of transition states, **8-TSta** and **8-TStb**, for this step are trigonal bipyramidal. S1 and S3 take the axial positions and S2, the carbonyl and the azide stay in the equatorial plane. In contrast to **7ta** and **7tb**, **9ta** is square-pyramidal with S1-Ni-S3 of 162.5° and **9tb** is trigonal-bipyramidal with S1-Ni-S3 of 118.7° (Figure 4 and Table 6). However, S2 and the carbonyl stay *trans* to each other in both **9ta** and **9tb** instead of *cis* as found in **7ta** and **7tb**.

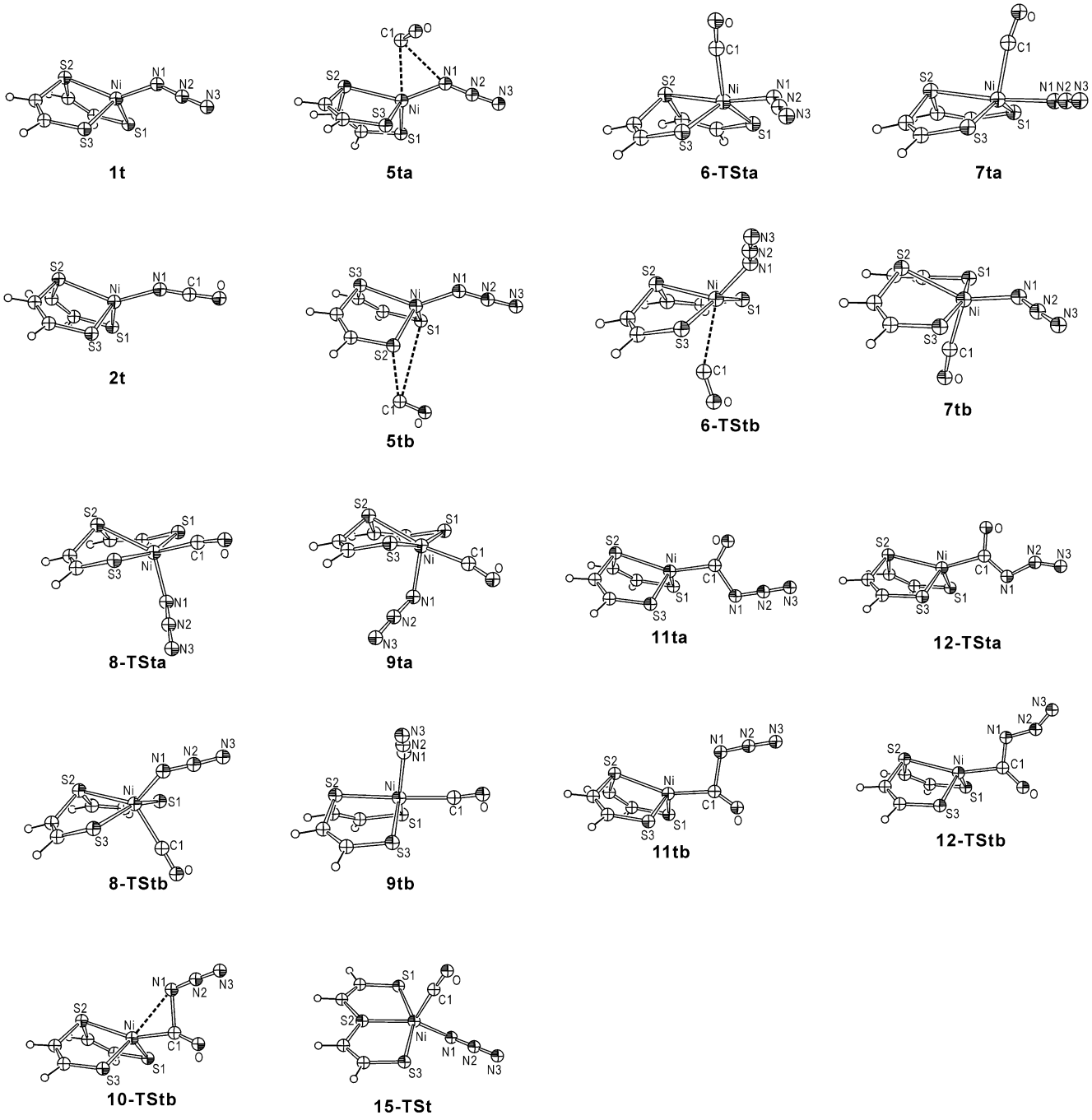

Figure 4. The B3LYP/BS-I geometries of the species in the triplet mechanism.

The activation enthalpy ($\Delta H^{\neq}$) for this step is 9.02 kcal mol^{-1} for the formation of **9ta** and 1.64 kcal mol^{-1} for that of **9tb**.

Third step: This step is similar to the second step in the singlet mechanism; the azide migrates from Ni to the carbonyl. However, the transition state **10-TSta**, which is in the direct pathway from **9ta** to **11ta**, is not located successfully after extensive searching, whereas the transition state **10-TStb**, between **9tb** and **11tb**, is found with an enthalpic barrier of 11.9 kcal mol^{-1}. Although the direct path has not been found, **9ta** can go to **11ta** by a detour. That is to say, **9ta** can transform to **9tb** by flattening and refolding the NiS_3 framework with an enthalpic barrier of 8 kcal mol^{-1}. Also **11tb** can easily change to **11ta** by rotating about the Ni–C bond.

Fourth step: Finally, the nickel carbonyl azide complexes, **11ta** and **11tb**, rearrange to produce product, the nickel isocyanate complex **2t**, by releasing a molecule of N_2 simultaneously. The transition states **12-TSta** and **12-TStb** are very early because of the exothermic formation of N_2

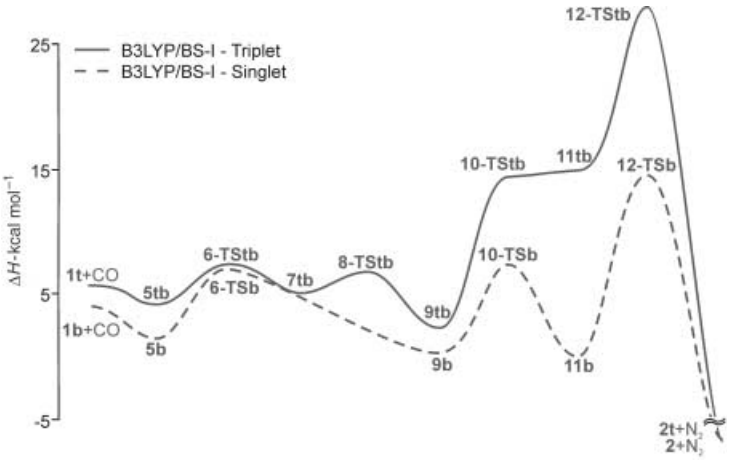

Figure 5. The comparison of the reaction coordinates of singlet and triplet mechanisms.

Comparison of closed-shell (singlet) and open-shell (triplet) mechanism

Based on experiments (X-ray crystals and NMR spectra), the reactants and products must be singlets. To compensate for the overestimation of the stability of triplets by the B3LYP functional, 10 kcal mol^{-1} were added to the enthalpy and free energy values of all triplet species. This addition brings the energies of the reactant and product into agreement with experimental evidence about the nature of the ground states.

As shown in Figure 5, the ΔH curves of singlet and triplet are close until the nickel carbonyl azide complexes (**9b** and **9tb**) are formed. The two states could mix together in this part of the mechanism. However, for the rearrangement of the carbonyl azide into isocyanate, the barrier for the triplet mechanism is much (~13 kcal mol^{-1} in enthalpy) higher than that for the singlet. Thus, triplet states might play a small role in the early stages of the reaction, but the singlet mechanism dominates in key steps such as in the rearrangement of carbonyl azide into isocyanate and N_2.

Further study of closed-shell (singlet) mechanismSingle-point energy (SPE) calculations based on the geometries optimized by B3LYP/BS-I: To ascertain the reliability of the DFT-B3LYP with basis sets (BS-I), larger basis sets (BS-II) are used to perform the SPE calculations. As listed in Table 7 and plotted in Figure 6, the larger basis sets (BS-II) just slightly increase the relative energies of the transition states. Because all species in our calculations are anionic and the solvent (THF) effect could be quite strong, the sol-

Table 7. Relative energies [kcal mol^{-1}] of singlet species based on the single-point energy (SPE) calculations[a] with BS-II, BP86, or solvent effect.

Species	B3LYP/BS-I	B3LYP/BS-II	B3LYP/BS-I(PCM)
1b + CO	4.90	3.33	2.83
5b	1.47	1.24	1.64
6-TSb	7.56	8.58	13.04
9b	−0.47	0.95	0.36
10-TSb	7.67	8.68	6.98
11b	−0.65	1.83	0.49
12-TSb	15.56	17.86	15.09
2 + N_2	−65.69	−68.25	−66.59

[a] All SPE are calculated on the optimized geometries with B3LYP/BS-I.

Table 6. B3LYP/BS-I structure parameters for triplet species in Figure 4.

Structure parameters[a]	**1t**	**5ta**	**6-TSta**	**7ta**	**8-TSta**	**9ta**	**11ta**	**12-TSta**	**15-TSt**
Ni−S2	2.486	2.475	2.570	2.576	2.645	2.489	2.515	2.515	2.285
Ni−S1	2.350	2.350	2.356	2.395	2.448	2.428	2.339	2.337	2.599
Ni−S3	2.350	2.355	2.399	2.370	2.427	2.422	2.340	2.337	2.562
Ni−N1	1.926	1.937	2.059	2.058	1.997	2.032	3.012	2.955	1.987
N1−N2	1.205	1.205	1.209	1.209	1.208	1.208	1.231	1.394	1.207
N2−N3	1.160	1.161	1.162	1.163	1.162	1.163	1.147	1.138	1.164
C1−N1		3.074	2.642	2.653	2.905	2.727	1.558	1.334	2.970
Ni−C1		3.095	2.060	2.021	1.993	2.057	2.005	2.001	1.952
C1−O		1.140	1.141	1.141	1.140	1.140	1.206	1.239	1.140
S2-Ni-N1	142.3	145.0	169.8	173.8	121.7	105.2			148.4
S2-Ni-C1		85.1	93.2	93.4	144.7	171.2	154.0	151.9	113.5
S1-Ni-S3	117.1	116.0	132.4	142.8	162.6	162.5	123.7	124.0	154.7
N1-N2-N3	176.9	176.7	176.2	176.2	175.7	175.7	179.4	145.6	176.0
Structure parameters[a]	**5tb**	**6-TStb**	**7tb**	**8-TStb**	**9tb**	**10-TStb**	**11tb**	**12-TStb**	**2t**
Ni−S2	2.478	2.423	2.474	2.555	2.496	2.495	2.505	2.520	2.485
Ni−S1	2.353	2.416	2.494	2.462	2.383	2.334	2.335	2.337	2.354
Ni−S3	2.348	2.404	2.479	2.481	2.396	2.333	2.335	2.337	2.354
Ni−N1	1.926	1.947	1.957	1.975	2.023	2.814	2.890	2.712	1.928
N1−N2	1.204	1.210	1.208	1.207	1.207	1.218	1.223	1.384	
N2−N3	1.161	1.160	1.161	1.163	1.162	1.158	1.153	1.138	
C1−N1	5.516	4.566	3.293	3.061	2.683	1.810	1.698	1.352	1.200
Ni−C1	4.242	2.801	2.026	2.030	2.128	2.010	2.012	2.022	
C1−O	1.139	1.143	1.141	1.140	1.140	1.175	1.185	1.225	1.202
S2-Ni-N1	141.2	126.0	149.1	127.2	96.2	116.6			143.3
S2-Ni-C1	96.4	86.3	99.2	133.1	176.5	156.5	156.9	159.5	
S1-Ni-S3	117.2	152.6	164.4	153.9	118.7	121.6	122.7	124.7	115.5
N1-N2-N3	176.8	175.7	175.9	176.0	176.4	177.0	177.0	146.8	

[a] Bond lengths in Å, bond angles in °.

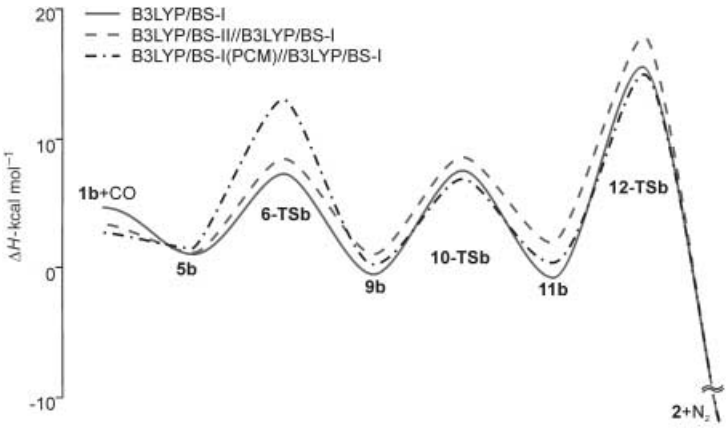

Figure 6. The reaction coordinates in the singlet mechanism.

vation energies are also calculated. Although the solvation energies are very large (~30 kcal mol^{-1} by PCM method), all species are nearly equally solvated, so relative energies are almost unchanged and the barriers are quite similar to those in vacuum (see Figure 6).

Conclusion

The flexibility of the $'S_3'^{2-}$ ligand developed by Sellmann and co-workers is essential for the low barriers predicted for this insertion/elimination reaction. Ni–S2 bond weakening is required for the successful attack of CO on Ni to form the pseudo five-coordinate intermediate **3** in the first step. The Ni–S2 bond strengthening then helps weaken the Ni–N bond and assist its migration to the carbonyl in the second step. In the last step, the loss of N_2 and the rearrangement of the carbonyl nitrene occur synchronously to produce the isocyanate complex. The release/then rebound of the S–Ni dative bond predicted for this mechanism could play an important role in metalloenzyme mechanisms as a means to open and close a coordination site.[25]

Acknowledgement

We thank the National Science Foundation (Grant No. CHE 9800184) and the Welch Foundation (Grant No. A-648) for their generous support.

[1] a) M. A. Halcrow, G. Christou, *Chem. Rev.* **1994**, *94*, 2421; b) A. F. Kolodziej, *Prog. Inorg. Chem.* **1994**, *41*, 493; c) M. J. Maroney, C. B. Allan, B. S. Chohan, S. B. Choundhury, Z. Gu, *ACS Symp. Ser.* **1996**, *653*, 74; d) C. A. Grapperhaus, M. Y. Darensbourg, *Acc. Chem. Res.* **1998**, *31*, 451; e) M. Y. Darensbourg, E. J. Lyon, J. J. Smee, *Coord. Chem. Rev.* **2000**, *206–207*, 533.

[2] a) D. Sellmann, S. Fünfgelder, G. Pöhlmann, F. Knoch, M. Moll, *Inorg. Chem.* **1990**, *29*, 4772; b) D. Sellmann, S. Fünfgelder, F. Knoch, M. Moll, *Z. Naturforsch. B* **1991**, *46*, 1601; c) D. Sellmann, H. Schillinger, F. Knoch, M. Moll, *Z. Naturforsch. B* **1992**, *47*, 748; d) D. Sellmann, W. Prechtel, F. Knoch, M. Moll, *Inorg. Chem.* **1993**, *32*, 538; e) D. Sellmann, D. Häußinger, F. Knoch, M. Moll, *J. Am. Chem. Soc.* **1996**, *118*, 5368; f) D. Sellmann, C. Allmann, F. W. Heinemann, F. Knoch, J. Sutter, *J. Organomet. Chem.* **1997**, *541*, 291–305.

[3] a) D. Sellmann, F. Geipel, F. W. Heinemann, *Chem. Eur. J.* **2000**, *6*, 4279; b) D. Sellmann, F. Geipel, F. Lauderbach, *Angew. Chem.* **2002**, *114*, 654; *Angew. Chem. Int. Ed.* **2002**, *41*, 632; c) D. Sellmann, F. Geipel, F. W. Heinemann, *Chem. Eur. J.* **2002**, *8*, 958; d) D. Sellmann, R. Prakash, F. Geipel, F. W. Heinemann, *Eur. J. Inorg. Chem.* **2002**, *8*, 2138; e) D. Sellmann, D. C. F. Blum, F. W. Heinemann, *Inorg. Chim. Acta* **2002**, *337*, 1.

[4] a) G. Musie, J. H. Reibenspies, M. Y. Darensbourg, *Inorg. Chem.* **1998**, *37*, 302; b) E. J. Lyon, I. P. Georgakaki, J. H. Reibenspies, M. Y. Darensbourg, *Angew. Chem.* **1999**, *111*, 3373; *Angew. Chem. Int. Ed.* **1999**, *38*, 3178; c) E. J. Lyon, I. P. Georgakaki, J. H. Reibenspies, M. Y. Darensbourg, *J. Am. Chem. Soc.* **2001**, *123*, 3268; d) X. Zhao, I. P. Georgakaki, M. L. Miller, R. Mejia-Rodriguez, C. Y. Chiang, M. Y. Darensbourg, *Inorg. Chem.* **2003**, *42*, 3917; e) X. Zhao, C. Y. Chiang, M. L. Miller, M. V. Rampersad, M. Y. Darensbourg, *J. Am. Chem. Soc.* **2003**, *125*, 518.

[5] M. J. Frisch, G. W. Trucks, H. B. Schlegel, G. E. Scuseria, M. A. Robb, J. R. Cheeseman, V. G. Zakrzewski, J. A. Montgomery, R. E. Stratmann, J. C. Burant, S. Dapprich, J. M. Millam, A. D. Daniels, K. N. Kudin, M. C. Strain, O. Farkas, J. Tomasi, V. Barone, M. Cossi, R. Cammi, B. Mennucci, C. Pomelli, C. Adamo, S. Clifford, J. Ochterski, G. A. Petersson, P. Y. Ayala, Q. Cui, K. Morokuma, D. K. Malick, A. D. Rabuck, K. Raghavachari, J. B. Foresman, J. Cioslowski, J. V. Ortiz, B. B. Stefanov, G. Liu, A. Liashenko, P. Piskorz, I. Komaromi, R. Gomperts, R. L. Martin, D. J. Fox, T. Keith, M. A. Al-Laham, C. Y. Peng, A. Nanayakkara, C. Gonzalez, M. Challacombe, P. M. W. Gill, B. G. Johnson, W. Chen, M. W. Wong, J. L. Andres, M. Head-Gordon, E. S. Replogle and J. A. Pople, Gaussian 98, Revision A.11.3; Gaussian, Inc., Pittsburgh, PA, **1998**.

[6] A. D. Becke, *J. Chem. Phys.* **1993**, *98*, 5648.

[7] C. Lee, W. Yang, R. G. Parr, *Phys. Rev. B* **1988**, *37*, 785.

[8] A. D. Becke, *Phys. Rev. A* **1988**, *38*, 3098.

[9] J. P. Perdew, *Phys. Rev. B* **1986**, *33*, 8822.

[10] R. G. Parr, W. Yang, *Density Functional Theory of Atoms and Molecules*, Oxford University Press, New York, **1989**.

[11] a) P. J. Hay, W. R. Wadt, *J. Chem. Phys.* **1985**, *82*, 270; b) W. R. Wadt, P. J. Hay, *J. Chem. Phys.* **1985**, *82*, 284.

[12] M. Couty, M. B. Hall, *J. Comput. Chem.* **1996**, *17*, 1359.

[13] A. W. Ehlers, M. Boehme, S. Dapprich, A. Gobbi, A. Hoellwarth, V. Jonas, K. F. Koehler, R. Stegmann, A. Veldkamp, G. Frenking, *Chem. Phys. Lett.* **1993**, *208*, 111.

[14] a) R. Ditchfield, W. J. Hehre, J. A. Pople, *J. Chem. Phys.* **1971**, *54*, 724; b) W. J. Hehre, R. Ditchfield, J. A. Pople, *J. Chem. Phys.* **1972**, *56*, 2257; c) P. C. Hariharan, J. Pople, A. *Mol. Phys.* **1974**, 27, 209; d) M. S. Gordon, *Chem. Phys. Lett.* **1980**, *76*, 163; e) P. C. Hariharan, J. Pople, A. *Theo. Chim. Acta.* **1973**, *28*, 213.

[15] a) K. Raghavachari, J. A. Pople, E. S. Replogle, M. Head-Gordon, *J. Phys. Chem.* **1990**, *94*, 5579; b) M. J. S. Dewar, C. H. Reynolds, *J. Comput. Chem.* **1986**, *7*, 140; c) A. D. McLean, G. S. Chandler, *J. Chem. Phys.* **1980**, *72*, 5639; d) R. Krishnan, J. S. Binkley, R. Seeger, J. A. Pople, *J. Chem. Phys.* **1980**, *72*, 650.

[16] M. Dolg, U. Wedig, H. Stoll, H. Preuss, *J. Chem. Phys.* **1987**, *86*, 866.

[17] a) S. Miertus, E. Scrocco, J. Tomasi, *Chem. Phys.* **1981**, *55*, 117; b) S. Miertus, J. Tomasi, *Chem. Phys.* **1982**, *65*, 239; c) M. Cossi, V. Barone, R. Cammi, J. Tomasi, *Chem. Phys. Lett.* **1996**, *255*, 327.

[18] J. P. Perdew, K. Burke, Y. Wang, *Phys. Rev. B* **1996**, *54*, 16533.

[19] J. P. Perdew, K. Burke, M. Ernzerhof, *Phys. Rev. Lett.* **1996**, *77*, 3865.

[20] a) L. Cavallo, H. Jacobsen, *Eur. J. Inorg. Chem.* **2003**, 892; b) S. P. de Visser, F. Ogliaro, P. K. Sharma, S. Shaik, *J. Am. Chem. Soc.* **2002**, *124*, 11809; c) S. P. de Visser, F. Ogliaro, N. Harris, S. Shaik, *J. Am. Chem. Soc.* **2001**, *123*, 3037d) N. Harris, S. Cohen, M. Filatov, F. Ogliaro, S. Shaik, *Angew. Chem.* **2000**, *112*, 2070; *Angew. Chem. Int. Ed.* **2000**, *39*, 2003; e) D. Schroder, S. Shaik, H. Schwarz, *Acc. Chem. Res.* **2000**, *33*, 139.

[21] O. Salomon, M. Reiher, B. A. Hess, *J. Chem. Phys.* **2002**, *117*, 4729.

[22] M. Reiher, O. Salomon, B. A. Hess, *Theor. Chem. Acc.* **2001**, *107*, 48.

[23] S. B. Boys, F. Bernardi, *Mol. Phys.* **1970**, *19*, 553.

[24] a) C. Gonzalez, H. B. Schlegel, *J. Chem. Phys.* **1989**, *90*, 2154; b) C. Gonzalez, H. B. Schlegel, *J. Phys. Chem.* **1990**, *94*, 5523.

[25] C. E. Webster, M. Y. Darensbourg, P. A. Lindahl, M. B. Hall, *J. Am. Chem. Soc.* **2004**, in press.

Received: February 11, 2003
Revised: December 18, 2003 [F4840]